7242 *Biochemistry* **2010,** *49,* 7242–7254
DOI: 10.1021/bi1008485

BIOCHEMISTRY
including biophysical chemistry & molecular biology
Current Topic

Elucidating the Catalytic Mechanism of Sulfite Oxidizing Enzymes Using Structural, Spectroscopic, and Kinetic Analyses[†]

Kayunta Johnson-Winters, Gordon Tollin,* and John H. Enemark*

Department of Chemistry and Biochemistry, The University of Arizona, Tucson, Arizona 85721

Received May 26, 2010; Revised Manuscript Received July 21, 2010

ABSTRACT: Sulfite oxidizing enzymes (SOEs) are molybdenum cofactor-dependent enzymes that are found in plants, animals, and bacteria. Sulfite oxidase (SO) is found in animals and plants, while sulfite dehydrogenase (SDH) is found in bacteria. In animals, SO catalyzes the oxidation of toxic sulfite to sulfate as the final step in the catabolism of the sulfur-containing amino acids, methionine and cysteine. In humans, sulfite oxidase deficiency is an inherited recessive disorder that produces severe neonatal neurological problems that lead to early death. Plant SO (PSO) also plays an important role in sulfite detoxification and in addition serves as an intermediate enzyme in the assimilatory reduction of sulfate. In vertebrates, the proposed catalytic mechanism of SO involves two intramolecular one-electron transfer (IET) steps from the molybdenum cofactor to the iron of the integral *b*-type heme. A similar mechanism is proposed for SDH, involving its molybdenum cofactor and *c*-type heme. However, PSO, which lacks an integral heme cofactor, uses molecular oxygen as its electron acceptor. Here we review recent results for SOEs from kinetic measurements, computational studies, electron paramagnetic resonance (EPR) spectroscopy, electrochemical measurements, and site-directed mutagenesis on active site residues of SOEs and of the flexible polypepetide tether that connects the heme and molybdenum domains of human SO. Rapid kinetic studies of PSO are also discussed.

In animals, sulfite oxidase (SO)[1] is a molybdenum cofactor-dependent enzyme that catalyzes the oxidation of sulfite to sulfate, using ferricytochrome *c* (cyt c_{ox}) as the physiological electron acceptor (eq 1) (*1*−*4*):

$$SO_3^{2-} + H_2O \rightarrow SO_4^{2-} + 2H^+ + 2e^- \quad (1)$$

This reaction is biologically essential, serving as the final step in the catabolism of sulfur-containing amino acids, cysteine and methionine. SO also functions in detoxifying exogenously supplied sulfite and sulfur dioxide.

The SO family is comprised of plant assimilatory nitrate reductases (NR) and sulfite oxidizing enzymes (SOEs) found in animals, plants, and bacteria. The SOEs include plant and animal SO and bacterial sulfite dehydrogenase (SDH). In animals, SO is located in the mitochondrial intermembrane space (*5*, *6*). Plant SO (PSO) is localized in the peroxisomes and does not react with cyt *c*; instead, PSO uses molecular oxygen as its terminal electron acceptor (*7*, *8*). SDH is located in the periplasm (*9*), and the enzyme from *Starkeya novella* is the most thoroughly characterized example.

SO is physiologically vital in human metabolism, and severe neurological damage and early childhood death result from deficiency of SO activity due to an inborn metabolic defect. The symptoms of inherited sulfite oxidase deficiency include dislocation of the ocular lenses, attenuated growth of the brain, and mental retardation (*10*, *11*). Other symptoms that have been reported in patients with SO deficiency include poor feeding, hypoactivity, dyspnea, diffuse edema, and seizures (*12*). The disease results either from molybdenum cofactor deficiency, which arises from a defect in its biosynthesis, or from certain point mutations within the SO enzyme (isolated SO deficiency) (*13*−*15*).

Prior to 2010, there had been no successful treatment for SO deficiency. Very recently, the case of an infant female patient, who was diagnosed with molybdenum cofactor deficiency at 6 days old, has been reported (*16*). The patient showed a homozygous G175R (GGG-to-AGG) change in exon 10 of the *MOCS1* gene, a mutation that disrupts the production of cyclic pyranopterin monophosphate (cPMP), a key step in the biosynthesis of the molybdenum cofactor (*16*−*18*). After substitution therapy with purified cyclic pyranopterin monophosphate (cPMP) (*13*), starting at 36 days old, all urinary metabolites of sulfite oxidase (sulfite, *S*-sulfocysteine, and thiosulfate) and xanthine oxidase deficiency (xanthine and uric acid) returned to almost normal readings and remained constant for more than one year. Thus, knowledge of the biosynthetic pathway of the molybdenum cofactor has made possible the first clinical treatment of SO deficiency. It is possible that an improved understanding of the catalytic

[†]This research was supported by National Institutes of Health Grant GM-037773 (to J.H.E.) and Ruth L. Kirchstein-National Institutes of Health Fellowship 1F32GM082136-01 (to K.J.-W.).

*To whom correspondence should be addressed. G.T.: phone, (520) 621-3447; fax, (520) 626-8065; e-mail, gtollin@u.arizona.edu. J.H.E.: phone, (520) 621-2245; fax, (520) 626-8065; e-mail, jenemark@u.arizona.edu.

[1]Abbreviations: SO, sulfite oxidase; SOEs, sulfite oxidizing enzymes; dRF, 5-deazariboflavin; DFT, density functional theory; EPR, electron paramagnetic resonance; SDH, sulfite dehydrogenase; NR, nitrate reductase; CSO, chicken sulfite oxidase; HSO, human sulfite oxidase; PSO, plant sulfite oxidase; cyt *c*, cytochrome *c*; IET, intramolecular electron transfer; k_{et}, electron transfer rate constant; K_{eq}, equilibrium constant for intramolecular electron transfer; k_f and k_r, microscopic rate constants for the forward and reverse directions, respectively, of intramolecular electron transfer; Moco, molybdopterin cofactor; *wt*, wild type; cPMP, cyclic pyranopterin monophosphate; *nqi*, nuclear quadrupole interaction; *hfi*, hyperfine interaction; *lpH*, low-pH; *hpH*, high-pH; P_i, phosphate-inhibited.

 Published on Web 07/28/2010

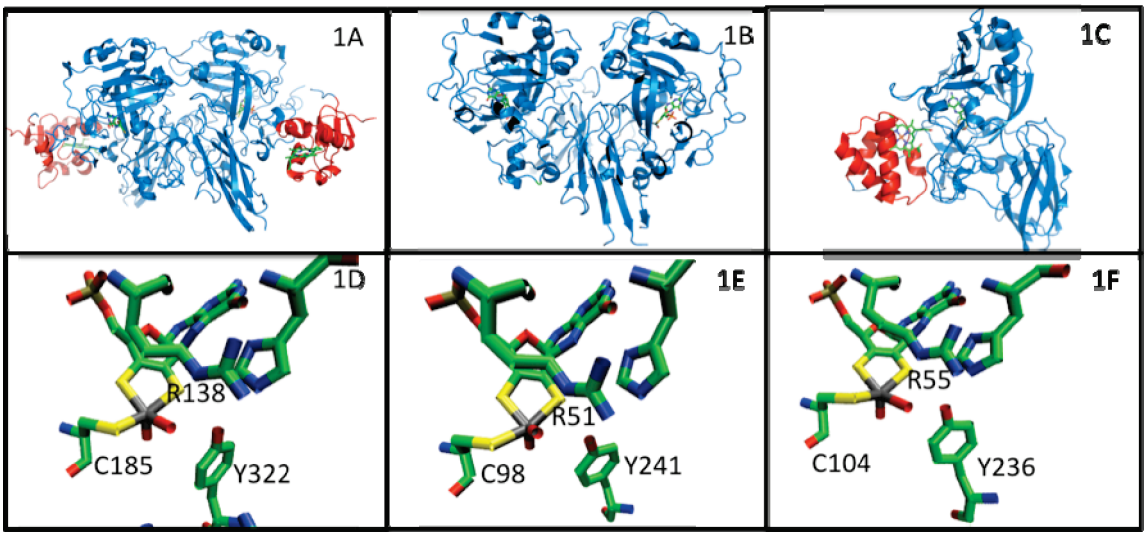

FIGURE 1: (A−C) Ribbon diagrams of the crystal structures of SOEs: (A) CSO (*26*), (B) PSO (*32*), and (C) SDH (*29*). Blue represents the molybdenum and C-terminal domain; red represents the heme domain. (D−F) Selected amino acid residues near the molybdenum active site of the corresponding SOEs of the top row.

mechanism of SOEs will result in additional treatment protocols for these disorders.

The development of recombinant human sulfite oxidase (HSO) has made it possible to prepare a library of mutations to study isolated SO deficiency, especially the effects of point mutations on the kinetic and spectroscopic properties of purified HSO (*19*−*23*). In a previous review, Feng and co-workers have discussed the effects of several mutations on the intramolecular electron transfer (IET) kinetics of SO (*24*). For example, three mutations that have been associated with SO deficiency in patients [HSO^{R160Q} (*21*), HSO^{G473D}, and HSO^{A208D} (*20*)] are near the active site of SO. Laser flash photolysis measurements of their IET rates showed that the k_{et} values were decreased by 3 orders of magnitude relative to that of the wild type. Thus, IET of these variants became rate-limiting and equal to the overall turnover rate (k_{cat}) determined from steady-state kinetic studies (*24*). Feng et al. also discussed several future research directions with regard to SO that still needed to be addressed. These topics included (1) studies of electron transfer, using SDH as a model; (2) the importance of the flexible tether connecting the heme and molybdenum domains in docking the two domains for electron transfer; (3) pulsed EPR experiments to elucidate the nature of the sulfite- and sulfate-bound and chloride-bound forms of SO; and (4) computational modeling and simulations to improve our understanding of chloride-bound SO and to improve our understanding of the role of specific amino acids in IET and SO catalysis. This review addresses these questions using molecular biology, rapid kinetics (laser flash photolysis and stopped-flow), advanced EPR spectroscopy, protein crystallography, and computational modeling.

STRUCTURAL MOTIF OF SULFITE OXIDIZING ENZYMES

Crystal structures for SO from *Arabidopsis thaliana* (*25*) and chicken liver (*26*) and SDH from *S. novella* (*27*) have been determined (Figure 1). In addition, structures of recombinant wild-type chicken SO (*wt* rCSO) proteins with and without sulfate bound and recombinant R138Q chicken SO ($rCSO^{R138Q}$) have been reported (*28*). Recently, structures of mutant forms of SDH have been determined (*29*−*31*) and will be discussed here.

Active Site. The molybdenum active site is buried within a positively charged pocket and has tyrosine, histidine, and arginine residues that are conserved throughout SOEs and plant assimilatory nitrate reductases and have direct interactions with sulfate in CSO (*26*). The molybdenum active sites exhibit similar square pyramidal geometry around the molybdenum atom (Figure 1). There is an axial terminal oxo group, and the equatorial plane has three sulfur atoms (two from the dithiolene moiety of the pyranopterin cofactor and one from a cysteine residue) and a water/hydroxo ligand.

Chicken Sulfite Oxidase (*CSO*). CSO is the only intact eukaryotic crystal structure determined to date and possesses both a heme and a molybdenum domain. It is a 110 kDa homodimer, and each subunit has three domains, an N-terminal b_5-type heme domain (Figure 1A, colored red), a central molybdenum binding domain, and a C-terminal interface domain (Figure 1A, colored blue) (*26*). The distance between the heme and molybdenum centers within this structure is ~32 Å. However, the b_5-type heme and the molybdenum domains are connected by a flexible polypeptide tether that varies in length, depending upon the SO species. CSO has a tether that contains 13 amino acids, whereas the tether in HSO is 14 amino acids in length [based upon sequence alignment (Figure 2)]. The sequence of the tether of CSO is very different from that of HSO.

The crystal structures reported for two forms of recombinant CSO (*wt* rCSO and $rCSO^{R138Q}$) contain only the C-terminal dimerization domain and the catalytic core domain, which houses the molybdenum cofactor center (*28*). Neither of these structures exhibits a heme domain. Superposition of the structures of *wt* rCSO and native CSO shows that they have nearly identical structures. Both the *wt* rCSO and $rCSO^{R138Q}$ SOEs were crystallized in the resting state (without sulfate) and with sulfate bound. *wt* rCSO contains two bound sulfates per monomer, whereas $rCSO^{R138Q}$ contains only one bound sulfate per monomer. The active site of SO has three positively charged residues, R138, R190, and R450, which are presumed to help guide the negatively charged substrate into the active site of the enzyme. The active site pocket of the sulfate-bound and resting state of the *wt* rCSO and $rCSO^{R138Q}$ forms showed significant changes in the position of R450, indicating that

```
CHICKEN SO   P-DEAPAAPDAQDP 96
HUMAN SO     PEDKVAPTVETSDP 118
```

FIGURE 2: Sequence alignment of the flexible tether regions of CSO and HSO. Amino acids highlighted in red are conserved between the two species, while those highlighted in blue are similar. Mutations discussed in this work are indicated in the HSO sequence. Proline residues mutated to alanines are in bold type, and deleted residues are underlined.

this residue undergoes a conformational change upon substrate binding.

Plant Sulfite Oxidase. The crystal structure of PSO reveals that this enzyme is a homodimer, with an overall fold similar to that of CSO. PSO has two domains, an N-terminal Moco and a C-terminal dimerization domain (*32*), with no additional heme domain (Figure 1B). The active site is positively charged and has the conserved Tyr-His-Arg motif found in CSO (Figure 1E). The purpose of SO in plants is to detoxify excess sulfite in the cell, preventing sulfitolysis, and to serve as an intermediate enzyme in the assimilatory reduction of sulfate (*33*).

Sulfite Dehydrogenase. Sulfite dehydrogenase is a heterodimer, containing both a molybdenum-binding subunit (SorA) and a smaller heme *c*-containing subunit (SorB) (*29*). The domains of the SorA subunit have the same overall fold as the Moco and dimerization domains of both CSO and PSO (Figure 1C). Unlike the eukaryotic CSO, SDH does not possess a flexible polypeptide tether. Also, the distance between the heme and molybdenum centers in bacterial SDH is shorter (~16 Å) than the distance found in CSO. The SorB subunit and the heme *b* domain of chicken liver SO have a similar overall shape. The crystal structures of the SDH^{Y236F} (*30*), SDH^{R55M}, and SDH^{H57A} (*31*) mutants of SDH have also been determined. Combining these results with those for *wt* SDH has enabled potential electron transfer pathways between the heme and molybdenum redox centers to be postulated and evaluated by steady-state kinetics (*31*) and laser flash photolysis measurements (*34*).

Structure of SDH^{R55M}. Within SDH^{wt}, the side chain of R55 occupies a space that is close to the substrate binding site, forming hydrogen bonds with the equatorial oxo ligand of the molybdenum cofactor, Gln33 OE1, and a water molecule. It also forms a salt bridge with propionate 6 of the heme moiety of the cytochrome subunit, which effectively locks the propionate group into the appropriate position for one of the proposed electron transfer pathways (*29*). However, within the SDH^{R55M} crystal structure, the side chain of M55 does not occupy the same space that R55 does in the *wt* structure. M55 bends away, packing into a small cavity between the side chains of L121 and Q33. The space previously occupied by R55 in SDH^{wt} is empty (Figure 3A) (*31*).

Structure of SDH^{H57A}. Kappler and co-workers found that the SDH^{H57A} structure confirms that the substitution of H57 with an alanine identifies an additional water molecule that sits within the proximity of the imidazole ring in SDH^{wt} (*31*). The water molecule is able to form hydrogen bonds with N5 and O4 of the molybdopterin cofactor. Like SDH^{Y236F}, SDH^{H57A} appears to have increased the mobility of the R55 side chain and the interacting propionate 6 side chain of the heme (*30*, *31*). Kappler and co-workers found that both Y236 and H57 are necessary to stabilize R55 in a position for optimal bonding of hydrogen to the heme 6-propionate (Figure 3B).

MECHANISM OF THE SULFITE OXIDIZING ENZYMES

The catalytic mechanism of animal sulfite oxidase, originally proposed by Hille (Figure 4) (*35*−*38*), has become widely accepted. The proposed mechanism of animal SO starts with the fully oxidized resting Mo(VI)/Fe(III) state. Two-electron oxidation of sulfite to sulfate occurs at the molybdenum center, which is reduced to Mo(IV). The first intramolecular electron transfer (IET) step occurs when the reduced Mo(IV) transfers one electron to the oxidized Fe(III) b_5 heme. The resultant Mo(V)/Fe(II) species contains a diamagnetic Fe(II) center and a paramagnetic $4d^1$ Mo(V) center which can be detected by electron paramagnetic resonance (EPR) spectroscopy (*39*−*42*) (see the following section). The Mo(V)/Fe(II) species transfers an electron to the physiological electron acceptor $(\text{cyt } c)_{ox}$, producing the Mo(V)/Fe(III) state. A second IET step generates the Mo(VI)/Fe(II) state, and reduction of a second molecule of cyt *c* regenerates the fully oxidized Mo(VI)/Fe(III) state of the enzyme. The portion of the catalytic mechanism in which the oxidized enzyme is reduced by two electrons and sulfate is produced is termed the reductive half-reaction. The oxidative half-reaction thus involves two one-electron transfers of electrons to cyt *c* to yield oxidized SO and two molecules of reduced cyt *c*.

EPR SPECTROSCOPY

The utility of EPR spectroscopy for investigating the Mo(V) sites of SOEs formed in the reductive half-reaction of Figure 4 has been recognized since the early 1980s, with the identification of three distinct continuous wave (CW) EPR forms of vertebrate SO: low-pH (*lpH*), high-pH (*hpH*), and phosphate-inhibited (P_i) (*43*−*45*). The coordination structures of the Mo(V) sites of SOEs obtained by pulsed EPR spectroscopy have been discussed previously (*46*), and the applications of pulsed EPR methods to SOEs have also been extensively reviewed (*47*). Therefore, only a few more recent EPR structural results for SOEs are presented here.

Bray and co-workers originally proposed that chloride and phosphate were directly coordinated to Mo(V) in the *lpH* and P_i forms, respectively, but no ^{35}Cl or ^{37}Cl ($I = {}^3/_2$) or ^{31}P ($I = {}^1/_2$) hyperfine interactions (*hfi*) were directly detected for these nuclei by CW EPR (*42*−*45*, *48*). In 1996, electron spin echo envelope modulation (ESEEM) studies between 8 and 18 GHz detected ^{31}P *hfi* for the P_i form of vertebrate SO and demonstrated that it has an equatorial monodentate phosphate group (*42*). However, until recently, the role of Cl^- in *lpH* SO remained elusive. A multifrequency CW EPR experiment using HSO and $^{35}Cl^-$- and $^{37}Cl^-$-enriched solutions showed very small spectral differences that were interpreted as indications of the presence of an axial Cl^- ligand *trans* to the terminal oxo group, but the limited resolution of the CW EPR spectra precluded reliable determination of the *hfi* and nuclear quadrupole interaction (*nqi*) parameters required to define the structure of *lpH* SO (*49*). Very recently, the magnetic resonance parameters of ^{35}Cl and ^{37}Cl ($I = {}^3/_2$) in *lpH* SO were finally measured by ESEEM methods, and density functional theory (DFT) calculations favored a structure in which the Cl^- anion is hydrogen bonded to the equatorial OH ligand and surrounded by several proton donors from nearby water molecules and charged amino acid side chains (*50*).

At some stage of the catalytic cycle of Figure 4, the product, SO_4^{2-}, has to be released from the active site. This release might occur from either the Mo(IV) or Mo(V) states of the reductive

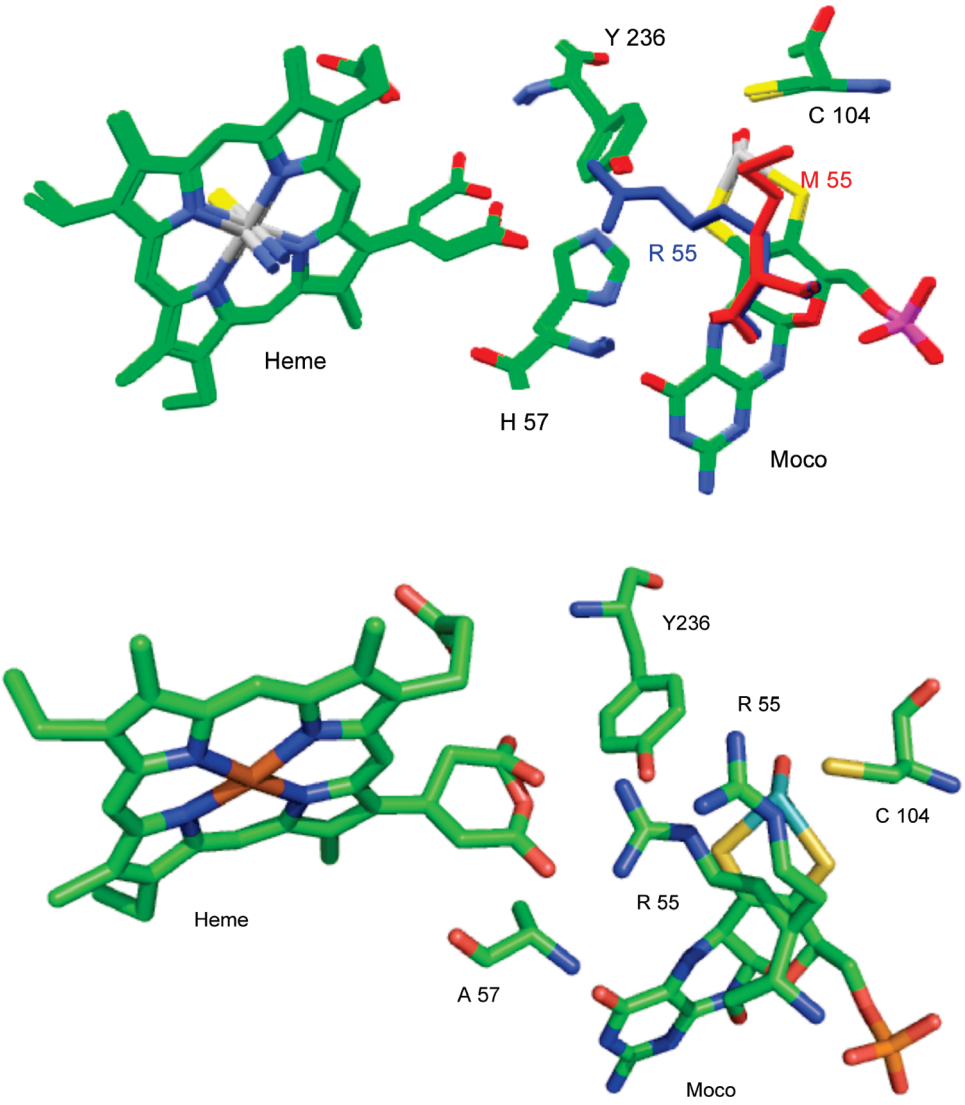

FIGURE 3: Superposition of the active site structures of SDH^{wt} and SDH^{R55M} (top), showing that the M55 side chain (red) in SDH^{R55M} does not occupy the same space as R55 (blue) in SDH^{wt}. M55 bends away, packing into a small cavity between the side chains of L121 and Q33, and the space previously occupied by R55 in SDH^{wt} is empty (*31*). Structure of the active site of SDH^{H57A} (bottom), showing the two disordered conformations of the R55 side chain (*31*).

half-reaction (Scheme 1). In 1982, Bray et al. reported that the presence of excess sulfite leads to another EPR-active Mo(V) species at low pH, which they attributed to a sulfite complex of the Mo center (*51*). Experimental evidence of a Mo(V) species with a sulfur-containing ligand was obtained only recently from pulsed EPR investigations of samples reduced with sulfite labeled with ^{33}S ($I = {}^{3}/_{2}$) at low pH, which allowed, for the first time, direct detection of coupling to ^{33}S. This coupling was initially observed in PSO from *A. thaliana* and was assigned to a Mo(V)−SO_4 complex (*52*). It was suggested that a conformational change of some of the nearby amino acid residues blocked hydrolysis of the sulfate ligand, and a structure similar to the P_i form was proposed (*42*), with a monodentate sulfate ligand (*52*). Subsequently, numerous examples of *blocked* forms have been observed for mutants of HSO and of SDH (*22*, *53*). More recently, it was shown that the *blocked* form is also produced in chloride-depleted samples of *wt* HSO. Addition of excess chloride to the *blocked* forms of SOEs converts them, at least partially, to the familiar *lpH* form (*54*).

The hydrolysis of the product (sulfate) with $H_2{}^{17}O$ in the reductive half-reaction (Figure 4) provides a convenient method for introducing ^{17}O ($I = {}^{5}/_{2}$) into the Mo(V) center of SOEs (*46*). It has long been known that the *lpH* and *hpH* forms show distinctly different ^{17}O *hfi* (*55*), but it was not possible to investigate the details of their *hfi* and *nqi* parameters prior to the development of high-resolution variable-frequency pulsed EPR spectrometers (*56*) and sophisticated DFT programs to relate experimental results to electronic and molecular structure (*57*, *58*). At high pH, SOEs exhibit two types of ^{17}O atoms in pulsed EPR experiments. One has a large *hfi* of ~30−40 MHz and can be associated with the equatorially coordinated O-containing ligand. The second has a much smaller *hfi* (~5−6 MHz). For *hpH* SO, this latter ^{17}O signal was assigned to the axial oxo−Mo(V) group from comparison to the results for model compounds and from extensive DFT calculations (*39*, *59*). At low pH (~6), the *blocked* forms of SOEs also exhibit two types of ^{17}O signals (*22*). The larger *hfi* (~18 MHz) is again associated with the equatorial O-containing ligand, but the origin of the smaller ^{17}O *hfi* (5−6 MHz) is less clear because its *nqi* value (~4−5 MHz) is substantially larger than those for known axial oxo ligands in model compounds (1.5 MHz) (*59*). For studies of *blocked* forms of SOEs in $H_2{}^{17}O$, it is also important to note that the oxygen

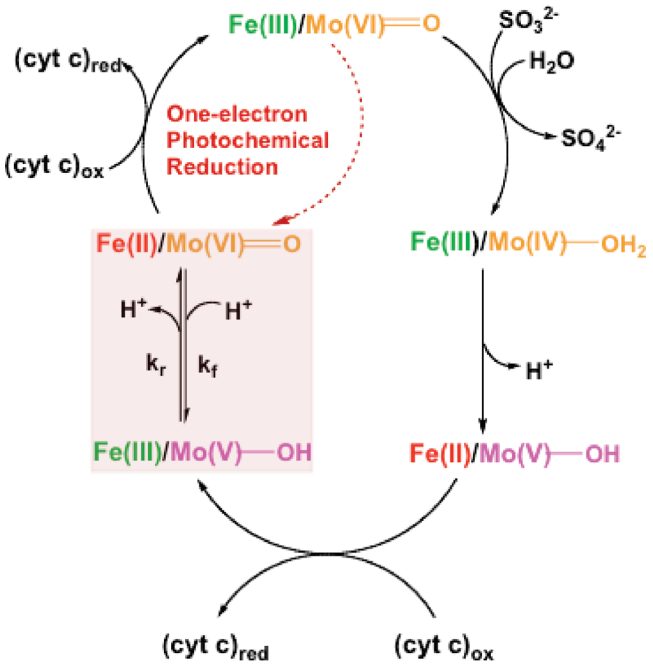

FIGURE 4: Proposed oxidation-state changes occurring at the Mo and Fe centers of animal SO during the catalytic oxidation of sulfite and the concomitant reduction of (cyt *c*)$_{ox}$.

Scheme 1: Possible Reaction Pathways for the Catalytic Oxidation of Sulfite by SDH or SO[a]

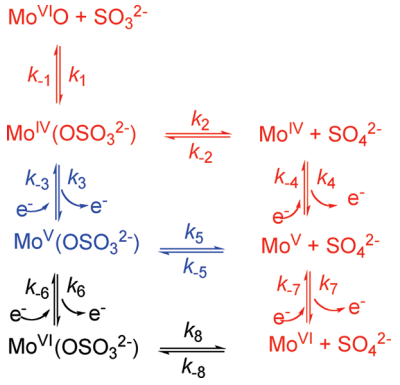

[a]For the sake of simplicity, the enzyme and substrate are depicted as $Mo^{VI}O$ and SO_3^{2-}, respectively. The pathways differ in the sequence of steps that transform the enzyme−substrate complex, $Mo^{IV}(OSO_3^{2-})$, into product (sulfate) and the reoxidized Mo(VI) state of the enzyme. The pathway colored red is the one commonly proposed, in which product release precedes reoxidation of the enzyme. For the pathway colored black, the enzyme−substate complex is oxidized by two electrons prior to product release (*34*). See the text for additional discussion.

atoms of sulfite exchange very rapidly (*60*). Consequently, all of the O atoms of a coordinated sulfite (reactant) or sulfate (product) anion will be labeled with ^{17}O in the reductive half-reaction of Figure 4. Recent extensive DFT calculations suggest that for the *blocked* form the smaller ^{17}O *hfi* arises from remote O atoms on the sulfite (or sulfate) group bound to Mo(V) (*61*). The DFT calculations for the sulfite-coordinated structure originally proposed by Bray et al. (*51*) give somewhat better agreement with the experimental *nqi* parameters for this weakly coupled ^{17}O and for the central ^{33}S atom compared to the sulfate-coordinated structure proposed previously by us (*52*). Figure 5 summarizes

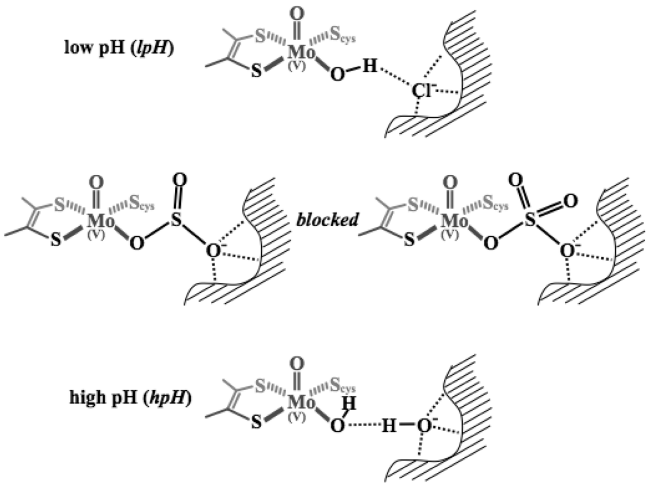

FIGURE 5: Proposed structures of the molybdenum active sites of SOEs from pulsed EPR experiments and DFT calculations for the *lpH* (*50*), *blocked* (*61*), and *hpH* forms (*58*). The *blocked* form shown on the left has bound reactant (sulfite); the form shown on the right has bound product (sulfate). See the text and ref *61* for details.

the current view of the structures of the *lpH*, *hpH*, and *blocked* forms of SOEs.

The availability of more than 4 million genome sequences from databases and more than 40000 protein structures from the Protein Data Bank (PDB) has made it possible to analyze protein folds of SOEs in all domains of life using bioinformatics (*62*, *63*). After multiple-sequence alignments, Dahl and Kappler determined a phylogenetic relationship with three distinguishable groups of SOEs (*63*). Group 1 includes the pathogen enzymes; group 2 contains the classic SOEs and nitrate reductases, and group 3 contains enzymes from *Archaea*, phototrophic and soil bacteria. Chicken, human, and plant SO along with SDH are all included in group 2. Members of this group contain a dimerization domain and a molybdenum domain (*26*, *29*, *32*).

Similar bioinformatic analyses performed by Weiner and coworkers identified an *Escherichia coli* protein, YedY, as a part of the SOE family (*62*, *63*). The crystal structure of YedY has been determined and has revealed that this protein has only the molydopterin binding SO fold (*64*). YedY is categorized in group 3. Its heme counterpart is a separate monoheme cytchrome *b* protein known as YedZ (*64*). To date, very little is known about the function of YedY. Sequence comparison of plant, chicken, nitrate reductase, *S. novella* SDH, and YedY reveals that there are 15 residues that are conserved throughout these five structures (*64*). One of these conserved residues is the molybdenum coordinating cysteine residue (*64*).

INTRAMOLECULAR ELECTRON TRANSFER (IET) KINETIC STUDIES IN SULFITE OXIDIZING ENZYMES

Intramolecular electron transfer (IET) is essential for the catalyzed reaction of SO. In animal SO and SDH, IET occurs between the heme and the molybdenum centers of the enzyme (Figure 4). The IET process can be studied using laser flash photolysis techniques. Laser flash photolysis experiments can be performed anaerobically in solutions containing 5-deazariboflavin (dRF) and freshly prepared semicarbazide or EDTA (AH_2) as a sacrificial reductant. It has been previously shown that dRF radicals are generated with a laser pulse and will then rapidly reduce the Fe(III) heme center of animal SO and *S. novella* SDH

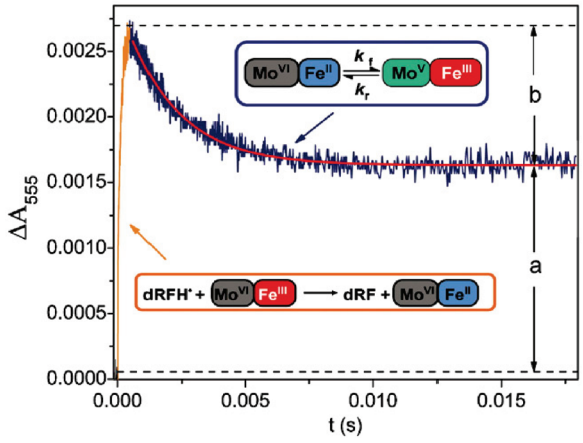

FIGURE 6: Kinetic transient obtained at 555 nm upon photoexcitation of a solution containing wild-type human SO, dRF, and 0.5 mM fresh semicarbazide hydrochloride (pH 7.4). The portion of the figure outlined by the orange box points to the initial heme reduction by dRFH•; this process is pseudo-first-order, and its rate depends on protein concentration. The dark blue box points to heme reoxidation due to the subsequent IET between the Mo and Fe centers; this process is independent of protein concentration, consistent with its intraprotein nature. The red solid line indicates a single-exponential fit to the IET phase. $K_{eq} = b/a$. Reproduced with permission from ref *24*. Copyright 2007 Elsevier B.V.

by one electron (Figures 4 and 6). This process corresponds to the reverse of the second physiologically essential IET step that is boxed in Figure 4. The initial rapid increase in absorbance at 555 nm is due to the reduction of the heme from the Fe(III) form to the Fe(II) form (eq 4) by the dRF radical. This process is followed by a slower absorption decay that is due to the net IET from the Fe(II) to Mo(VI), i.e., the intramolecular reoxidation of Fe(II) [forming the Fe(III)/Mo(V) species (eq 5)]. The laser flash photolysis technique follows the IET process in the reverse direction of the enzymatic turnover.

The methodologies used to obtain rate and equilibrium constants for IET in SO have been described previously (*65*) and are summarized below. The laser flash photolysis apparatus system has been extensively described (*66*) as has been the basic photochemical process by which 5-deazariboflavin semiquinone (dRFH•) is generated by the reaction between triplet-state dRF and the sacrificial reductant and used to reduce redox-active proteins (eqs 2−5) (*67*−*69*).

$$\mathrm{dRF} \xrightarrow{h\nu} {}^{1}\mathrm{dRF} \rightarrow {}^{3}\mathrm{dRF} \tag{2}$$

$${}^{3}\mathrm{dRF} + \mathrm{AH_2} \rightarrow \mathrm{dRFH^{\bullet}} + \mathrm{AH^{\bullet}} \tag{3}$$

$$\mathrm{dRFH^{\bullet}} + \mathrm{Mo(VI)/Fe(III)} \rightarrow \mathrm{dRF} + \mathrm{Mo(VI)/Fe(II)} \tag{4}$$

$$\mathrm{Mo(VI)/Fe(II)} \underset{k_r}{\overset{k_f}{\rightleftharpoons}} \mathrm{Mo(V)/Fe(III)} \tag{5}$$

The IET rate constant can be calculated by fitting the heme reoxidation curve with an exponential function (eq 6) where the IET rate constant is the sum of the forward and reverse electron transfer rate constants (k_f and k_r, respectively, in eq 7).

$$\frac{dA_{555}}{dt} = a + b\exp(-k_{et}t) \tag{6}$$

$$k_{et} = d_f + k_r \tag{7}$$

The equilibrium constant can then be calculated using the parameters *a* and *b*, which are determined from the kinetic traces. A_0 is the absorbance extrapolated to time zero, assuming that the photochemically induced reduction of SO is instantaneous.

$$a = A_0\frac{k_r}{k_{et}} = A_0\frac{k_r}{k_f + k_r} \tag{8}$$

$$b = A_0\frac{k_f}{k_{et}} = A_0\frac{k_f}{k_f + k_r} \tag{9}$$

$$K_{eq} = \frac{k_f}{k_r} = \frac{b}{a} \tag{10}$$

The forward and reverse rate constants (k_f and k_r, respectively) of IET can then be calculated from the equilibrium constant (eq 10), thereby providing quantitative information about interdomain electron transfer in the enzyme. Note that k_f in these flash photolysis experiments is actually the reverse of the net physiological IET direction.

Tether Linking the Heme and Molybdenum Domains of SO: Past and Recent Studies. Until recently, little has been known about the role of the tether within animal SO (Figure 2), and this linkage is not present in plant or bacterial SOEs. The initial work on this tether was performed by Feng and co-workers and has been discussed previously (*24*, *70*). They proposed that interdomain motion that decreases the Mo to Fe distance is essential for rapid IET and that the flexible tether linking the two domains of SO facilitates this motion. Consistent with this, laser photolysis revealed that the IET rate constant in CSO decreased with an increase in solvent viscosity. Steady-state kinetics and EPR measurements on SO were also consistent with this hypothesis (*70*).

Kawatsu and Beratan have used a computational model to explore the mechanisms of IET in proteins such as SO, in which domains containing two cofactors are linked by a flexible tether (*71*). They found that the constrained conformational flexibility of the tether introduces an entropic component to the effective donor−acceptor interaction potential that produces a kinetic regime intermediate between "unimolecular" and "bimolecular". Their calculations predicted that for SO the tether length may control the transition between the electron tunneling and diffusion-limited regimes. Recently, Pushie and George used molecular dynamics calculations to investigate the large-scale domain motions of CSO (*72*). They observed motion of the N-terminal heme domain into an orientation similar to that postulated for rapid electron transfer. The simulations also probed the dynamics of specific active site residues in an attempt to improve our understanding of the structural and thermodynamic details of SO (*72*). Very recently, Utesch and Mroginski investigated the interdomain motion of CSO by combining steered molecular dynamics with all-atom molecular dynamics (*73*). They obtained a stable three-dimensional "docked" structure with a relatively short Mo···Fe distance (~19 Å), similar to that proposed previously from the rapid IET rates measured experimentally (*24*, *65*). The best theoretically calculated IET pathways for the docked model involved one to three interfacial water molecules and gave IET rates that were within 1 order of magnitude of the experimental values.

Prior to 2010, there were no experimental data from site-specific mutants for investigating the role of conformational changes of the tether that had been proposed from the effects of

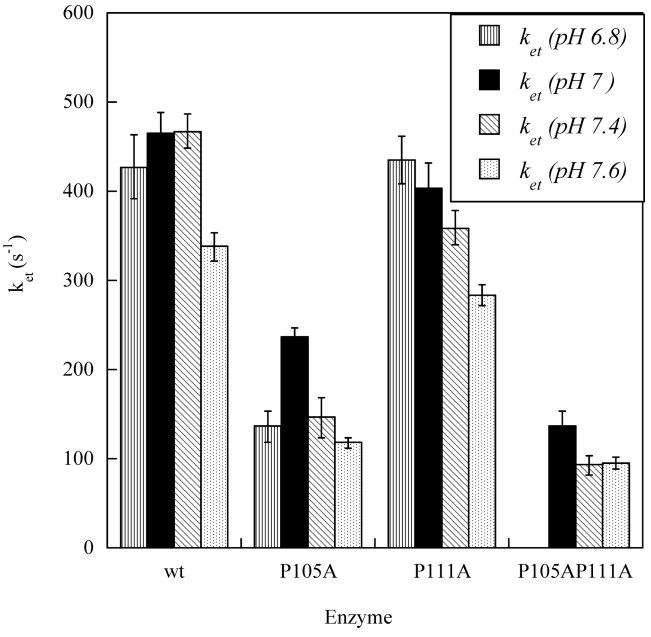

FIGURE 7: IET rate constants for the proline to alanine tether mutants (*79*).

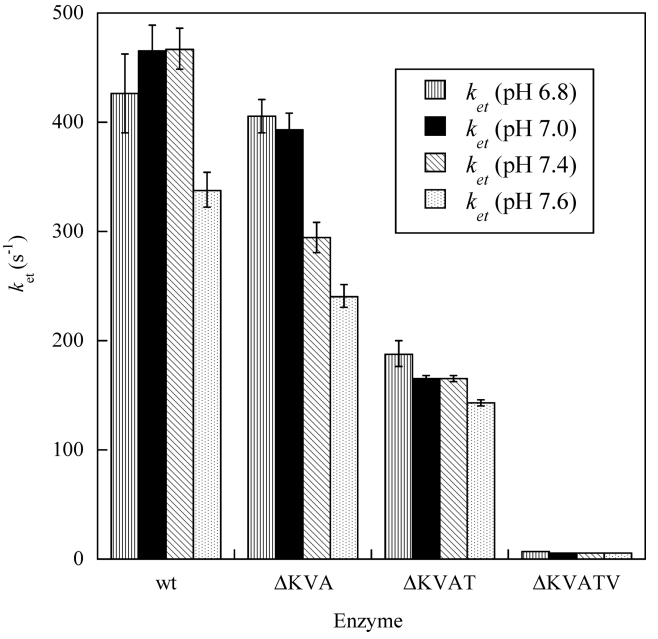

FIGURE 8: IET rate constants for tether deletion mutants (*79*).

viscosity on IET (*70*) and from theoretical calculations (*71*). Recently, the proposed roles of the tether in facilitating conformational change and reactivity have been explored by altering both the length and flexibility of the tether in HSO by site-specific mutagenesis, and the reactivities of the resulting variants were studied using laser flash photolysis and steady-state kinetics assays (*79*).

To change the flexibility of the tether, two conserved proline residues were mutated to alanines, P105 (adjacent to the heme domain) and P111 (at the center of the tether) (Figure 2). The double mutant, P105A/P111A, has also been made. While P105 is conserved within CSO and HSO, P111 is not. However, P111 is conserved within other mammalian forms. Figure 7 illustrates the dependence of k_{et} on pH and mutation. The data show that the P105A mutation decreases k_{et} by approximately 3-fold at pH 7.4. In contrast, the P111A mutation has an only minimal effect on k_{et}. The IET rate constants for the P105A/P111A double mutant are similar to those for P105A, suggesting that the P105A change is the primary cause of the decrease in the level of IET that is observed in this mutant.

The equilibrium constants (K_{eq}) for the P111A mutant show a pH dependence with a trend that is similar to that of the wild type; i.e., K_{eq} increases with an increase in pH. However, this trend is not seen with P105A. The kinetic data indicate that the P111A mutation in the middle of the tether has little effect on the IET kinetics. However, the much stronger effects on the IET kinetics for the P105A mutation suggest that this conserved proline, which is adjacent to the heme domain, promotes a tether conformation that results in optimal IET.

In addition to these proline to alanine mutations, several nonconserved residues [K108, V109, A110, T112, and V113 (Figure 2)] have been deleted from the tether to determine the effects of tether length on the IET kinetics of HSO. Deletions of three [ΔK108V109A110 (ΔKVA)], four [ΔK108V109A110T112 (ΔKVAT)], and five [ΔK108V109A110T112V113 (ΔKVATV)] nonconserved amino acids from the tether result in steadily decreasing IET rate constants, from 467 ± 19 s^{-1} in *wt* HSO to 5.59 ± 0.03 s^{-1} in ΔKVATV HSO at pH 7.4 (Figure 8). Interestingly, the largest decrease occurs upon deletion of the fifth residue (ΔKVATV). Additionally, all three deletion mutants exhibited decreasing IET rates with an increase in pH from 6.8 to 7.6. K_{eq} was significantly larger for ΔKVATV HSO (0.91 ± 0.03) in comparison to the *wt* HSO value (0.46 ± 0.02) and those of the other tether deletion mutants, but all the enzymes have a maximal K_{eq} around pH 7.4. To improve our understanding of the cause of this large increase in K_{eq} for ΔKVATV, spectroelectrochemistry studies were performed on *wt* and ΔKVATV HSO (Table 1), which will be discussed in the spectroelectrochemistry section.

The steady-state kinetics revealed that the largest effect observed was on the Michaelis−Menten constants (K_m) for P111A and P105A/P111A, which were approximately 5-fold higher than for the wild-type value (data not shown). The increase in K_m caused a 30% decrease in the catalytic efficiency (k_{cat}/K_m) of the enzyme. From these results, we concluded that the P111A mutation may affect the binding of sulfite to the enzyme. In addition, the steady-state data revealed that the k_{cat} values for each of these mutations are much smaller than k_{et}. Therefore, the IET process is not rate-limiting in catalysis, which is also true of the *wt* enzyme.

The steady-state kinetic parameters for ΔKVA and ΔKVAT HSO are slightly higher in comparison to that of *wt* HSO. However, the turnover number for ΔKVATV HSO (10.6 ± 0.3 s^{-1}) is approximately one-third of that of the wild type (26.9 ± 0.5) at pH 8.0. Unlike the proline to alanine mutations, IET for the ΔKVATV deletion mutant became rate-limiting during catalysis. Thus, decreasing the length of the tether apparently influences the docking of the heme domain onto the molybdenum domain, thereby changing the distance and relative orientation of the two redox centers. This effect is the probable cause for the decrease in k_{et}.

Very recently, the tether sequence of CSO (Figure 2) was introduced into HSO. The expectation was that this chimeric HSO protein would show IET kinetics that were faster than those of *wt* HSO and more similar to those of CSO. Surprisingly, however, IET for the chimeric HSO was actually slower than that for *wt* HSO (*74*). This result suggests that the composition of the

Table 1: Electrochemical Midpoint Potentials of SOE Cofactors[a]

	HSO	CSO	SDH	P105A HSO	ΔKVATV HSO
pH	7.5	7.5	7.1	7.5	7.5
heme cofactor [Fe(III/II)]	62 ± 2^c (*79*)	$\sim 69^d$ (*78*)	177^d (*82*)	56 ± 3^c (*79*)	42 ± 2^c (*79*)
molybdenum cofactor (VI/V)	41 ± 1^b (*79*)	not determined	264^d (*82*)	36 ± 1^b (*79*)	41 ± 1^b (*79*)

[a]All potentials are in millivolts vs the standard hydrogen electrode. [b]Calculated from $\Delta E^{\circ}_{\text{reaction(heme-Mo)}}$ and the experimental heme potential. [c]Determined by spectroelectrochemistry (see Figure 9). [d]Determined by protein film voltammetry.

nonconserved tether sequence of animal SOs may have become optimized for individual species. The kinetic results for all of the tether mutants point to a critical role for the tether in facilitating the IET reaction between the heme and molybdenum centers.

Mechanistic Considerations Based upon Conserved Arginine Residues in the Active Sites of SOEs. A new analysis of possible mechanistic pathways of sulfite oxidizing enzymes has emerged from laser flash photolysis and EPR studies on *wt* SDH and its R55 variants (*34*). Three variants of SDH (R55M, R55Q, and R55K) were made to explore the role of R55 in the pathway for IET in SDH. The SDH^{R55Q} variant had the same Arg to Gln substitution that is observed in R160Q in humans, which is a fatal mutation, causing sulfite oxidase deficiency. HSO^{R160Q} shows a substantial decrease in the level of IET, which is almost 400-fold lower than that of *wt* HSO ($122 \pm 5\ s^{-1}$) (*21*). For SDH^{R55Q}, the laser flash photolysis data revealed that k_{et} was 3-fold larger than that for SDH^{wt}. Both K_{eq} and k_{et} were mildly pH-dependent within SDH^{R55Q}. At pH 5.1, there was a 2-fold increase in K_{eq} for this variant (*34*).

The IET rate constant for SDH^{R55K} was unchanged with a varying pH, which is similar to the trend for SDH^{wt}. However, the IET rate could not be determined at pH 6.0. IET in SDH^{R55K} is much slower ($15 \pm 0.7\ s^{-1}$) than in SDH^{wt}. Between pH 5.1 (0.59 ± 0.02) and 5.5 (0.34 ± 0.03), the SDH^{R55K} variant showed a decrease in K_{eq}. These data are much different from those for HSO^{R160K}, which showed a decrease in the level of IET.

In the SDH^{R55M} variant, the hydrogen bonding interactions within the active site are disrupted. The IET rate constant for SDH^{R55M} ($217 \pm 25\ s^{-1}$) was 2-fold larger than that for SDH^{wt} ($122 \pm 5\ s^{-1}$) at pH 6 and increased 4-fold (535 ± 44) by pH 5.1. While the IET rate constant for SDH^{R55M} was pH-dependent, K_{eq} was nearly pH-independent. These behaviors are the opposite of those observed for SDH^{wt}. Therefore, both the forward and reverse IET rate constants for SDH^{R55M} increase with a decrease in pH, raising the possibility that SDH^{R55M} has a more efficient tunneling pathway for IET (*21*, *34*).

The structure of SDH^{R55M} shows that there is a sulfate anion bound within the active site, which is different from the case for SDH^{wt}, SDH^{Y236F} (*30*), or SDH^{H57A} (*31*). The pulsed EPR studies of SDH^{R55M} show only a *hpH*-type signal, similar to that of the SDH^{wt} enzyme, with no pH dependence (*53*). SDH^{R55Q} exhibits the *blocked* form, with bound sulfate at low pH, which was verified by ^{33}S couplings observed upon reduction with ^{33}S-labeled sulfite (*53*). This *blocked* feature has also been observed in the fatal mutant, HSO^{R160Q} (*22*).

SDH^{R55M} and SDH^{R55Q} are the first SOE active site variants to display an increase in the IET rate constant. This effect is the opposite of that observed in HSO^{R160Q} (*21*). These results indicate that the conserved arginine within the active site of SOEs is not a required part of the electron transfer pathway between the heme and molybdenum domains. However, the result is consistent with the positively charged arginine influencing the docking between the two domains in animal SO. Additional kinetic studies of SDH catalysis have shown that the R55 residue is important for effective substrate binding, and that $K_{Msulfite,app}$ for SDH^{R55M} is 2−3 orders of magnitude larger than that for SDH^{wt} (*31*). This result is also consistent with that data for SDH^{R55K}, which showed a $K_{Msulfite,app}$ factor ~10 times larger than that for SDH^{wt} (*31*).

On the basis of the kinetic data and the pulsed EPR studies of SDH^{wt} and variants, and similar studies on HSO^{R160Q}, alternative mechanistic possibilities for the catalytic cycle of SOEs must be considered. Scheme 1, proposed by Emesh et al., summarizes alternative possibilities for the catalytic cycle of SOEs (*34*). The sequence colored red is the prevailing view (*1*, *24*, *75*), in which product is released (k_2) from the enzyme−substrate complex. This is followed by two sequential one-electron oxidations of the Mo center (k_4 and k_7). This mechanism was discussed previously above (see Figure 4).

A second alternative (colored blue) would be for the enzyme−substrate complex to be oxidized by one electron (k_3 in Scheme 1). This is followed by product dissociation (k_5) and then another oxidation by one electron (k_7). Emesh et al. suggested that this pathway is operative in SDH^{wt} and the R55 variants because IET is significantly faster than catalytic turnover (*34*). Direct evidence of the one-electron-oxidized enzyme−substrate complex, i.e., the $Mo^{V}(OSO_3^{2-})$ species of Scheme 1, has been obtained by pulsed EPR studies of HSO^{R160Q} that has been reduced by sulfite labeled with ^{33}S ($I = {}^3/_2$) (*22*) and other *blocked* forms of SOEs (*31*, *52*, *53*).

A third possibility colored black in Scheme 1 is that the enzyme−substrate complex is oxidized by two electrons back to the resting-state Mo(VI) (k_3 and k_6) before release of sulfate (k_8). The IET and steady-state kinetics of the SDH^{Y236F} variant are consistent with this pathway. This variant is catalytically competent even though it does not exhibit IET by laser flash photolysis (steps k_7 and k_{-7}) (*30*).

KINETICS OF PLANT SO

Hille and co-workers have recently reported in-depth rapid kinetics and steady-state studies of PSO, using stopped-flow methods. The data demonstrated that superoxide is produced during the course of the reaction between the reduced enzyme and molecular oxygen and then decays to hydrogen peroxide (*76*). The rate constant was linearly dependent on the concentration of molecular oxygen, and the second-order rate constant (k_{ox}) equaled $(8.7 \pm 0.5) \times 10^4\ M^{-1}\ s^{-1}$. They also found that the reaction in the presence of cyt *c* was biphasic, with a fast phase and a slow phase. This result indicated that the first equivalent of superoxide was generated from the rapid one-electron oxidation of the fully reduced Mo(IV) state to Mo(V). This reaction was followed by the slower oxidation of the Mo(V) state to the Mo(VI) state.

ELECTROCHEMISTRY

Studies of Animal SO. As discussed above, SO is a multidomain enzyme, containing heme and molybdenum redox centers. An extensive microcoulometric study of native CSO by Spence et al. investigated the reduction potentials of the Fe(III/II), Mo(VI/V), and Mo(V/IV) couples as a function of pH and anions in the medium (*77*). The Fe(III/II) couple was nearly independent of pH, whereas the Mo(VI/V) couple showed a pH dependence of ~60 mV per pH unit, characteristic of an accompanying proton transfer. More recently, Elliott et al. investigated native CSO by protein film voltammetry (PFV) (*78*). A catalytic current was observed in the "potential domain" of CSO upon addition of sulfite. From the limiting current, they obtained a turnover number (k_{cat}) of 2−4 s^{-1}, which is significantly slower than the reported turnover numbers of SO in solution (100 s^{-1}) (*38*). The PFV data suggested that a large fraction of the SO molecules immobilized on the electrode surface do not engage in catalysis but undergo noncatalytic electron transfer. The observed behavior is independent of the electrode and does not seem to be an artifact of the surface−protein interaction. The midpoints of the catalytic waves (E_{mid}) in the PFV experiments show a very small pH dependence, which is only consistent with the wave arising from action at the Fe(III/II) center (*77*) and identifies it as the central distributive site for catalytic ET. The redox potential at pH 7.5 is approximately 65 mV versus the standard hydrogen electrode, which is similar to the heme potential of *wt* HSO determined from spectroelectrochemistry (see the discussion below) (*79*).

The reduction potential of the b_5 heme of *wt* and mutant HSO has recently been measured using spectroelectrochemistry, following procedures described previously for heme proteins (*77*, *79*−*81*). Because the ratio of oxidized to reduced forms of each redox species is directly related to the absorbances of the optical spectra via Beer's law (assuming the extinction coefficients of the reduced and oxidized species are different at the chosen wavelength), the change in absorbance with respect to applied potential can be fit to the Nernst equation (eq 11) using the nonlinear least-squares fitting algorithm in Origin.

$$E_{app} = E^{\circ} + 2.303(RT/nF)\log_{10}([Ox]/[Red]) \qquad (11)$$

where E_{app} is the applied potential, $E°$ is the midpoint potential determined from these data, and [Ox] and [Red] are the concentrations of the Fe(III) and Fe(II) states, respectively, of the b_5 heme of HSO.

On the basis of the kinetic results of Johnson-Winters et al. (*79*), the laser flash photolysis data for ΔKVATV resulted in K_{eq} values that were approximately 0.91, compared to 0.46 for the wild type. To confirm whether this was a result of the change in the midpoint potential between the heme and molybdenum, spectroelectrochemistry studies were performed to determine the Fe(III/II) potentials for *wt* and ΔKVATV HSO. The corresponding midpoint potentials versus the standard hydrogen electrode are 62 ± 2 mV for *wt* HSO and 44 ± 2 mV for ΔKVATV HSO (Figure 9 and Table 1). Thus, the Fe(III/II) potential for ΔKVATV HSO is 18 ± 3 mV more negative than the *wt* value, supporting the laser flash photolysis kinetic data and favoring the Fe(III)/Mo(V) species in eq 5. Using the K_{eq} value from the laser flash photolysis data and the heme potential, the potential of the molybdenum center can be calculated, as well. The calculated potentials of the Mo(VI)/Mo(V) couple for ΔKVATV and *wt* HSO are 41 ± 2 and 42 ± 2 mV, respectively (Table 1). Therefore,

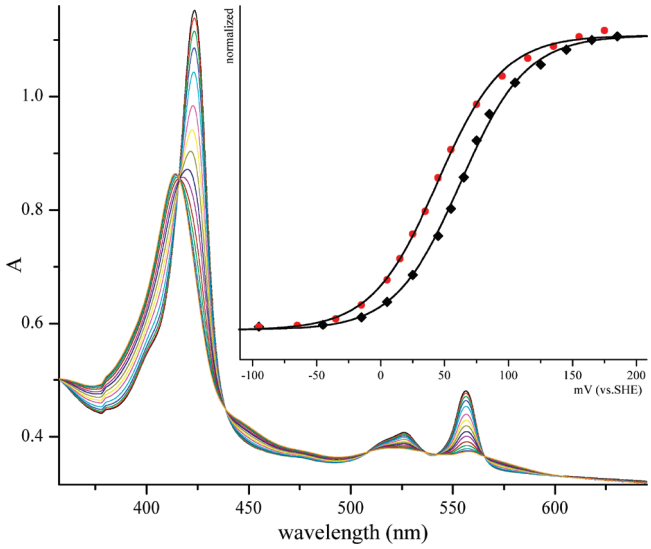

FIGURE 9: Spectroelectrochemical titration of the b_5 heme of wild-type HSO at pH 7.5 and 27 °C (*79*). The inset shows the fit of the data to eq 11 at 413 nm (*78*): black for the wild type and red for ΔKVATV.

it was concluded that the change in K_{eq} for ΔKVATV was primarily due to a change in the potential of the heme. Perhaps the deletion of five amino acids from the tether changes the exposure of the heme to solvent, thereby causing a shift in the potential and in K_{eq}.

Spectroelectrochemistry has also been used to measure the Fe(III/II) potential of the P105A mutant which shows much slower rates of IET compared to the wild type, but similar K_{eq} values (Figure 7). Table 1 shows that the Fe(III/II) potential for P105A is essentially identical to that of the wild type, as is the calculated Mo(VI/V) potential. Thus, the P105A mutation does not change the thermodynamic driving force for IET (as seen from K_{eq}) or the individual potentials of the two redox centers. Therefore, the 2−4-fold decrease in k_{et} for the P105A mutant compared to the *wt* value (Figure 7) presumably reflects differences in their IET pathways.

Studies of SDH. From PFV studies of SDH^{wt} on a pyrolytic graphite working electrode, McEwan and co-workers identified the heme and molybdenum potentials as follows: $E_{m,8}$[Fe(III/II)] = 177 mV, $E_{m,8}$[Mo(VI/V)] = 211 mV, and $E_{m,8}$[Mo(V/IV)] = −118 mV versus the standard hydrogen electrode (*82*). The Michaelis−Menten constant (K_m) for SDH^{wt} obtained upon saturation of the catalytic current with sulfite was similar to previous steady-state assay values (26 μM) (*13*). Also, using square wave voltammetry, they were able to show that the SDH^{wt} potentials of the heme and molybdenum exhibit a pH dependence.

Attempts to extend the PFV measurements to the SDH^{R55} variants, however, were not successful (*34*). Also, it was not feasible to directly determine the Mo(VI/V) potentials of the SDH^{R55} variants by EPR titrations, because of the large amount of protein required for such experiments. However, the Mo(VI/V) potentials of SDH^{wt} can be calculated by using K_{eq} (1.57 at pH 5.2) from the laser flash photolysis experiments and the Fe(III/II) potential determined from spectroelectrochemistry, as described above for HSO. For SDH^{wt}, this procedure gave a $\Delta E°$ of 12 mV and a calculated Mo(VI/V) potential of 196 mV (*34*). This calculated Mo(VI/V) potential is very different from the value of 381 mV reported for the direct experimental measurement for SDH^{wt} at pH 5.2 by PFV (*82*). It is unknown why these potential values vary by so much. However, it could be due to the fact that

Scheme 2: Overview of the Current State of Research on Sulfite Oxidizing Enzymes[a]

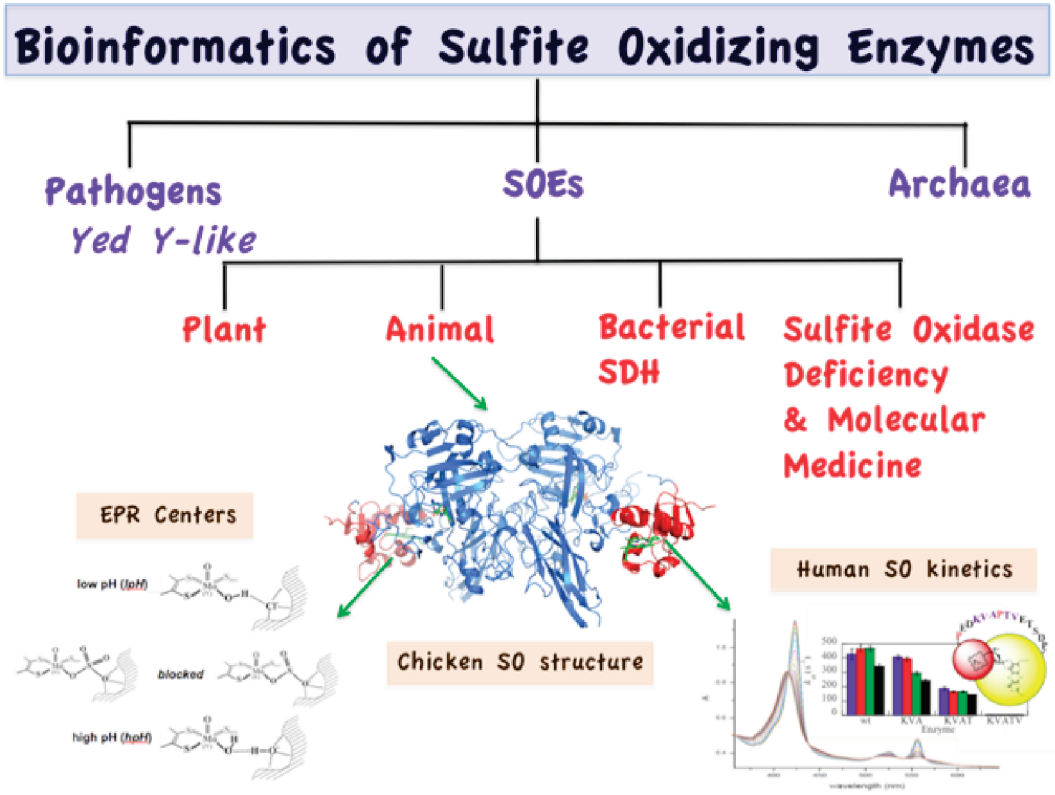

[a]From bioinformatic analyses, the diverse sulfite oxidase family of proteins that contains the same molybdenum cofactor center (*1*) can be classified into at least three groups (*63*, *85*). This review has focused on the SOEs. Animal sulfite oxidases possess two redox-active domains and present fundamental biophysical problems relating to intramolecular electron transfer (IET), the relationship of IET rates to steady-state kinetics, the overall conformation of the protein, and the molecular dynamics of the motion of the two domains relative to one another. The effects of extensive mutations of the tether connecting the heme and molybdenum domains of human SO have been discussed here. However, there are no X-ray structural results of the intact protein for any of these variants. The detailed structures of the molybdenum centers of these variants have been determined from analysis of high-resolution pulsed EPR spectra of their Mo(V) states as a function of pH, anions in the media, and mutations of nearby amino acid residues. A long-term hope is that these studies will contribute to the continuing development of molecular medicine for the treatment of sulfite oxidase deficiency (*13*, *16*).

the technique of PFV requires adsorption of the protein on an electrode surface and immobilization within a surfactant film. This is very different from the spectroelectrochemical determination of the potential in solution (*34*).

CONCLUSIONS

As noted above, a review of SOEs in 2007 by Feng and coworkers (*24*) and co-workers concluded with a list of topics to be addressed in future research in this area. Substantial progress has already been made on several of these topics by the combined approaches of molecular biology, rapid kinetics, advanced spectroscopy, protein crystallography, and computational modeling. Scheme 2 summarizes the current status of research on SOEs and some of the remaining challenges. Specifically, recent advances include the following.

(1) Flash photolysis studies of variants of HSO and of bacterial SDH have provided new insights concerning the amino acids involved in direct IET through the protein medium. In humans, the HSO^{R160Q} mutation is fatal, and the rate of IET in the purified protein is dramatically reduced relative to that of *wt* HSO. However, the analogous SDH^{R55Q} mutation of the conserved active site arginine in bacterial SDH does not decrease the rate of IET. In SDH, the heme and Mo domains are locked in place by strong interactions between the two subunits, whereas in HSO, the heme and Mo domains are linked by a flexible tether and domain reorientation is required to accomplish IET. These combined flash photolysis results suggest that in HSO the primary role of the positively charged R160 residue is to aid in docking the heme domain with the Mo domain for efficient IET and catalysis (*34*). The relative unimportance of R55 in SDH implies that this conserved active site arginine is not directly on the pathway for IET. Calculations of the IET pathway(s) for SDH should provide further insight concerning this hypothesis.

(2) Substantial progress has been made in elucidating the effect of the tether linking the heme and Mo domains of HSO on the rates of IET and steady-state kinetics. We have shown that both the length and composition of the tether strongly affect the rate of IET (*79*). Theoretical calculations of the effects of interdomain motion on IET are beginning to appear (*71*), and the first molecular mechanics calculations on the time evolution of the structure of CSO have recently been described (*72*, *73*). The increasing availability of GPU-based computer clusters should make molecular mechanics calculations of longer time trajectories of interdomain motions in SO more computationally tractable in the future (*83*). This is critical because IET occurs on the millisecond time scale, which is presently computationally inaccessible.

(3) Pulsed EPR spectroscopy of "difficult" nuclei (^{17}O, ^{33}S, ^{35}Cl, and ^{37}Cl) with $I > {}^1/_2$ has been combined with DFT calculations to elucidate the structures of the Mo(V) states of SOEs and to gain insight concerning their catalytic mechanisms.

The long-standing question of the structure of the *lpH* form of SO has been resolved via ^{35}Cl and ^{37}Cl pulsed EPR and DFT calculations; the chloride ion is in the second coordination sphere and hydrogen-bonded to the equatorial Mo-OH group and surrounding water molecules and proton donors from amino acid side chains (*50*). Observation of ^{33}S couplings in SOEs reduced by ^{33}S-labeled sulfite at low pH in chloride-depleted solutions has shown that the *blocked* form is a common Mo(V) species in SOEs. Addition of excess chloride converts the *blocked* form to the *lpH* form in most cases (*54*). DFT calculations on models for ^{33}S- and ^{17}O-labeled *blocked* SO suggest that a structure with O-bound sulfite is most likely. The weakly coupled ^{17}O atom detected in the blocked form is assigned to remote oxygen atoms of the sulfite (sulfate) ligand (*61*). Detection of the *nqi* parameters for strongly coupled equatorial ^{17}O ligands remains difficult, but recent advances in W-band ESEEM methods hold promise for future advances (*84*).

(4) X-ray crystal structures of several variants of SDH (*30*, *31*) have appeared, and structures of the Mo domain of recombinant CSO and CSO^{R138Q} have been described (*28*). However, to date the only structure of an intact form of vertebrate SO is the original report of native CSO at 1.9 Å resolution (*26*). The crystallization and structure determination of recombinant HSO, both *wt* and mutants, remain as challenges for future research on SO.

ACKNOWLEDGMENT

We thank Drs. Andrei Astashkin, Robert E. Berry, Changjian Feng, James T. Hazzard, Russ Hille, Ulrike Kappler, Eric L. Klein, Arnold Raitsimring, and Asha Rajapakshe, Mr. Robert Byrne, and Ms. Safia Emesh for helpful discussions.

REFERENCES

1. Hille, R. (1996) The Mononuclear Molybdenum Enzymes. *Chem. Rev. 96*, 2757–2816.
2. Rajagopalan, K. V., and Johnson, J. L. (2002) Sulfite Oxidase. In Wiley Encyclopedia of Molecular Medicine (Creighton, T. E., Ed.) pp 3048−3051, Wiley, New York.
3. Kisker, C. (2001) Sulfite Oxidase. In Handbook of Metalloproteins (Messerschmidt, A., Huber, R., Poulos, T., and Wieghardt, K., Eds.) pp 1121−1135, Wiley, New York.
4. Schindelin, H., Kisker, C., and Rajagopalan, K. V. (2001) Molybdopterin from Molybdenum and Tungsten Enzymes. *Adv. Protein Chem. 58*, 47–94.
5. Cohen, H. J., Betcher-Lange, S., Kessler, D. L., and Rajagopalan, K. V. (1972) Hepatic Sulfite Oxidase. Congruency in Mitochondria of Prosthetic Groups and Activity. *J. Biol. Chem. 247*, 7759–7766.
6. Kessler, D. L., Johnson, J. L., Cohen, H. J., and Rajagopalan, K. V. (1974) Visualization of Hepatic Sulfite Oxidase in Crude Tissue Preparations by Electron Paramagnetic Resonance Spectroscopy. *Biochim. Biophys. Acta 334*, 86–96.
7. Eilers, T., Schwarz, G., Brinkmann, H., Witt, C., Richter, T., Nieder, J., Koch, B., Hille, R., Hansch, R., and Mendel, R. R. (2001) Identification and Biochemical Characterization of *Arabidopsis thaliana* Sulfite Oxidase. A New Player in Plant Sulfur Metabolism. *J. Biol. Chem. 276*, 46989–46994.
8. Hansch, R., Lang, C., Riebeseel, E., Lindigkeit, R., Gessler, A., Rennenberg, H., and Mendel, R. R. (2006) Plant Sulfite Oxidase as Novel Producer of H_2O_2: Combination of Enzyme Catalysis With a Subsequent Nonenzymatic Reaction Step. *J. Biol. Chem. 281*, 6884–6888.
9. Kappler, U., Bennett, B., Rethmeier, J., Schwarz, G., Rainer-Deutzmann, R., McEwan, A. G., and Dahl, C. (2000) Sulfite:Cytochrome *c* oxidoreductase from *Thiobacillus novellus*. Purification, Characterization, and Molecular Biology of a Heterodimeric Member of the Sulfite Oxidase Family. *J. Biol. Chem. 275*, 13202–13212.
10. Johnson, J. L. (2003) Prenatal Diagnosis of Molybdenum Cofactor Deficiency and Isolated Sulfite Oxidase Deficiency. *Prenatal Diagn. 23*, 6–8.
11. Dublin, A. B., Hald, J. K., and Wootton-Gorges, S. L. (2002) Isolated Sulfite Oxidase Deficiency: MR Imaging Features. *Am. J. Neuroradiol. 23*, 484–485.
12. Sass, J. O., Gunduz, A., Araujo, C., Funayama, R., Korkmaz, B., Giselle, K., Pinto, D., Tuysuz, B., Lam, C.-W., Reiss, J., Walter, M., Yalcinkaya, C., and Camelo Junior, J. S. (2010) Functional Deficiencies of Sulfite Oxidase: Differential Diagnoses in Neonates Presenting with Intractable Seizures and Cystic Encephalomalacia. *Brain Dev. 32*, 544–549.
13. Schwarz, G., Santamaria-Araujo, J. A., Wolf, S., Lee, J. H., Adham, I. M., Grone, H. J., Schwegler, H., Sass, J. O., Otte, T., Hanzelmann, P., Mendel, R. R., Engel, W., and Reiss, J. (2004) Rescue of Lethal Molybdenum Cofactor Deficiency by a Biosynthetic Precursor from *Escherichia coli*. *Hum. Mol. Genet. 13*, 1249–1255.
14. Matthies, A., Rajagopalan, K. V., Mendel, R. R., and Leimkuhler, S. (2004) Evidence for the Physiological Role of a Rhodanese-Like Protein for the Biosynthesis of the Molybdenum Cofactor in Humans. *Proc. Natl. Acad. Sci. U.S.A. 101*, 5946–5951.
15. Johnson, J. L., and Duran, M. (2001) Molybdenum Cofactor Deficiency and Isolated Sulfite Oxidase Deficiency, pp 3163−3177, McGraw-Hill, New York.
16. Veldman, A., Santamaria-Araujo, J. A., Sollazzo, S., Pitt, J., Gianello, R., Yaplito-Lee, J., Wong, F., Ramsden, C. A., Reiss, J., Cook, I., Fairweather, J., and Schwarz, G. (2010) Successful Treatment of Molybdenum Cofactor Deficiency Type A with cPMP. *Pediatrics 125*, e1249–e1254.
17. Johnson, J. L., Waud, W. R., Rajagopalan, K. V., Duran, M., Beemer, F. A., and Wadman, S. K. (1980) Inborn Errors of Molybdenum Metabolism: Combined Deficiencies of Sulfite Oxidase and Xanthine Dehydrogenase in a Patient Lacking the Molybdenum Cofactor. *Proc. Natl. Acad. Sci. U.S.A. 77*, 3715–3719.
18. Mendel, R. R., and Bittner, F. (2006) Cell Biology of Molybdenum. *Biochim. Biophys. Acta 1763*, 621–635.
19. Temple, C. A., Graf, T. N., and Rajagopalan, K. V. (2000) Optimization of Expression of Human Sulfite Oxidase and its Molybdenum Domain. *Arch. Biochem. Biophys. 383*, 281–287.
20. Feng, C., Wilson, H. L., Tollin, G., Astashkin, A. V., Hazzard, J. T., Rajagopalan, K. V., and Enemark, J. H. (2005) The Pathogenic Human Sulfite Oxidase Mutants G473D and A208D are Defective in Intramolecular Electron Transfer. *Biochemistry 44*, 13734–13743.
21. Feng, C., Wilson, H. L., Hurley, J. K., Hazzard, J. T., Tollin, G., Rajagopalan, K. V., and Enemark, J. H. (2003) Essential Role of Conserved Arginine 160 in Intramolecular Electron Transfer in Human Sulfite Oxidase. *Biochemistry 42*, 12235–12242.
22. Astashkin, A. V., Johnson-Winters, K., Klein, E. L., Feng, C., Wilson, H. L., Rajagopalan, K. V., Raitsimring, A. M., and Enemark, J. H. (2008) Structural Studies of the Molybdenum Center of the Pathogenic R160Q Mutant of Human Sulfite Oxidase by Pulsed EPR Spectroscopy and ^{17}O and ^{33}S Labeling. *J. Am. Chem. Soc. 130*, 8471–8480.
23. Wilson, H. L., Wilkinson, S. R., and Rajagopalan, K. V. (2006) The G473D Mutation Impairs Dimerization and Catalysis in Human Sulfite Oxidase. *Biochemistry 45*, 2149–2160.
24. Feng, C., Tollin, G., and Enemark, J. H. (2007) Sulfite Oxidizing Enzymes. *Biochim. Biophys. Acta 1774*, 527–539.
25. Hille, R. (2003) Plants have SOX: The Structure of Sulfite Oxidase from *Arabidopsis thaliana*. *Structure 11*, 1189–1190.
26. Kisker, C., Schindelin, H., Pacheco, A., Wehbi, W. A., Garrett, R. M., Rajagopalan, K. V., Enemark, J. H., and Rees, D. C. (1997) Molecular Basis of Sulfite Oxidase Deficiency from the Structure of Sulfite Oxidase. *Cell 91*, 973–983.
27. Kappler, U., and Bailey, S. (2004) Crystallization and Preliminary X-ray Analysis of Sulfite Dehydrogenase from *Starkeya novella*. *Acta Crystallogr. D60*, 2070–2072.
28. Karakas, E., Wilson, H. L., Graf, T. N., Xiang, S., Jaramillo-Busquets, S., Rajagopalan, K. V., and Kisker, C. (2005) Structural Insights into Sulfite Oxidase Deficiency. *J. Biol. Chem. 280*, 33506–33515.
29. Kappler, U., and Bailey, S. (2005) Molecular Basis of Intramolecular Electron Transfer in Sulfite-Oxidizing Enzymes is Revealed by High Resolution Structure of a Heterodimeric Complex of the Catalytic Molybdopterin Subunit and a *c*-Type Cytochrome Subunit. *J. Biol. Chem. 280*, 24999–25007.
30. Kappler, U., Bailey, S., Feng, C., Honeychurch, M. J., Hanson, G. R., Bernhardt, P. V., Tollin, G., and Enemark, J. H. (2006) Kinetic and Structural Evidence for the Importance of Tyr236 for the Integrity of the Mo Active Site in a Bacterial Sulfite Dehydrogenase. *Biochemistry 45*, 9696–9705.

31. Bailey, S., Rapson, T., Johnson-Winters, K., Astashkin, A. V., Enemark, J. H., and Kappler, U. (2009) Molecular Basis for Enzymatic Sulfite Oxidation: How Three Conserved Active Site Residues Shape Enzyme Activity. *J. Biol. Chem. 284*, 2053–2063.
32. Schrader, N., Fischer, K., Theis, K., Mendel, R. R., Schwarz, G., and Kisker, C. (2003) The Crystal Structure of Plant Sulfite Oxidase Provides Insights into Sulfite Oxidation in Plants and Animals. *Structure 11*, 1251–1263.
33. Hänsch, R., Lang, C., Rennenberg, H., and Mendel, R. R. (2007) Significance of Plant Sulfite Oxidase. *Plant Biol. 9*, 589–595.
34. Emesh, S., Rapson, T. D., Rajapakshe, A., Kappler, U., Bernhardt, P. V., Tollin, G., and Enemark, J. H. (2009) Intramolecular Electron Transfer in Sulfite-Oxidizing Enzymes: Elucidating the Role of a Conserved Active Site Arginine. *Biochemistry 48*, 2156–2163.
35. Hille, R. (1999) Molybdenum Enzymes. *Essays Biochem. 34*, 125–137.
36. Hille, R. (1994) The Reaction Mechanism of Oxomolybdenum Enzymes. *Biochim. Biophys. Acta 1184*, 143–169.
37. Brody, M. S., and Hille, R. (1995) The Reaction of Chicken Liver Sulfite Oxidase with Dimethylsulfite. *Biochim. Biophys. Acta 1253*, 133–135.
38. Brody, M. S., and Hille, R. (1999) The Kinetic Behavior of Chicken Liver Sulfite Oxidase. *Biochemistry 38*, 6668–6677.
39. Astashkin, A. V., Feng, C., Raitsimring, A. M., and Enemark, J. H. (2005) ^{17}O ESEEM Evidence for Exchange of the Axial Oxo Ligand in the Molybdenum Center of the High pH Form of Sulfite Oxidase. *J. Am. Chem. Soc. 127*, 502–503.
40. Astashkin, A. V., Raitsimring, A. M., Feng, C., Johnson, J. L., Rajagopalan, K. V., and Enemark, J. H. (2002) Pulsed EPR Studies of Nonexchangeable Protons Near the Mo(V) Center of Sulfite Oxidase: Direct Detection of the α-Proton of the Coordinated Cysteinyl Residue and Structural Implications for the Active Site. *J. Am. Chem. Soc. 124*, 6109–6118.
41. Astashkin, A. V., Mader, M. L., Pacheco, A., Enemark, J. H., and Raitsimring, A. M. (2000) Direct Detection of the Proton-Containing Group Coordinated to Mo(V) in the High pH Form of Chicken Liver Sulfite Oxidase by Refocused Primary ESEEM Spectroscopy: Structural and Mechanistic Implications. *J. Am. Chem. Soc. 122*, 5294–5302.
42. Pacheco, A., Basu, P., Borbat, P., Raitsimring, A. M., and Enemark, J. H. (1996) Multifrequency ESEEM Spectroscopy of Sulfite Oxidase in Phosphate Buffer: Direct Evidence for Coordinated Phosphate. *Inorg. Chem. 35*, 7001–7008.
43. Lamy, M. T., Gutteridge, S., and Bray, R. C. (1980) Electron-Paramagnetic-Resonance Parameters of Molybdenum(V) in Sulphite Oxidase from Chicken Liver. *Biochem. J. 185*, 397–403.
44. Gutteridge, S., Lamy, M. T., and Bray, R. C. (1980) The Nature of the Phosphate Inhibitor Complex of Sulphite Oxidase from Electron-Paramagnetic-Resonance Studies Using Oxygen-17. *Biochem. J. 191*, 285–288.
45. Bray, R. C., Gutteridge, S., Lamy, M. T., and Wilkinson, T. (1983) Equilibria Amongst Different Molybdenum (V)-Containing Species from Sulphite Oxidase. Evidence for a Halide Ligand of Molybdenum in the Low-pH Species. *Biochem. J. 211*, 227–236.
46. Enemark, J. H., Astashkin, A. V., and Raitsimring, A. M. (2006) Investigation of the Coordination Structures of the Molybdenum(V) Sites of Sulfite Oxidizing Enzymes by Pulsed EPR Spectroscopy. *Dalton Trans.,* 3501–3514.
47. Enemark, J. H., Astashkin, A. V., and Raitsimring, A. M. (2010) High Resolution EPR Spectroscopy of Mo-Enzymes. Sulfite Oxidases: Structural and Functional Implications. In Biological Magnetic Resonance Volume 29. Metals in Biology: Applications of High Resolution EPR to Metalloenzymes (Hanson, G. R., and Berliner, L. J., Eds.) pp 121−168, Springer, New York.
48. Bray, R. C. (1988) The Inorganic Biochemistry of Molybdoenzymes. *Q. Rev. Biophys. 21*, 299–329.
49. Doonan, C. J., Wilson, H. L., Bennett, B., Prince, R. C., Rajagopalan, K. V., and George, G. N. (2008) Mo(V) Electron Paramagnetic Resonance of Sulfite Oxidase Revisited: The Low-pH Chloride Signal. *Inorg. Chem. 47*, 2033–2038.
50. Klein, E. L., Astashkin, A. V., Ganyushin, D., Riplinger, C., Johnson-Winters, K., Neese, F., and Enemark, J. H. (2009) Direct Detection and Characterization of Chloride in the Active Site of the Low-pH Form of Sulfite Oxidase Using Electron Spin Echo Envelope Modulation Spectroscopy, Isotopic Labeling, and Density Functional Theory Calculations. *Inorg. Chem. 48*, 4743–4752.
51. Bray, R. C., Lamy, M. T., Gutteridge, S., and Wilkinson, T. (1982) Evidence from Electron-Paramagnetic-Resonance Spectroscopy for a Complex of Sulphite Ions With the Molybdenum Centre of Sulphite Oxidase. *Biochem. J. 201*, 241–243.
52. Astashkin, A. V., Johnson-Winters, K., Klein, E. L., Byrne, R. S., Hille, R., Raitsimring, A. M., and Enemark, J. H. (2007) Direct Demonstration of the Presence of Coordinated Sulfate in the Reaction Pathway of *Arabidopsis thaliana* Sulfite Oxidase Using ^{33}S labeling and ESEEM Spectroscopy. *J. Am. Chem. Soc. 129*, 14800–14810.
53. Rapson, T. D., Astashkin, A. V., Johnson-Winters, K., Bernhardt, P. V., Kappler, U., Raitsimring, A. M., and Enemark, J. H. (2010) Pulsed EPR Investigations of the Mo(V) Centers of the R55Q and R55M Variants of Sulfite Dehydrogenase from *Starkeya novella*. *J. Biol. Inorg. Chem. 15*, 505–514.
54. Rajapakshe, A., Johnson-Winters, K., Nordstrom, A. R., Meyers, K. T., Emesh, S., Astashkin, A. V., and Enemark, J. H. (2010) *Biochemistry 49*, 5154–5159.
55. Cramer, S. P., Johnson, J. L., Rajagopalan, K. V., and Sorrell, T. N. (1979) Observation of ^{17}O Effects on Mo(V) EPR Spectra in Sulfite Oxidase, Xanthine Dehydrogenase, and $MoO(SC_6H_5)_4^-$. *Biochem. Biophys. Res. Commun. 91*, 434–439.
56. Astashkin, A. V., Enemark, J. H., and Raitsimring, A. M. (2006) 26.5−40 GHz K_a-band pulsed EPR spectrometer. *Concepts Magn. Reson., Part B 29B*, 125–136.
57. http://www.thch.uni-bonn.de/tc/orca.
58. Astashkin, A. V., Klein, E. L., Ganyushin, D., Johnson-Winters, K., Neese, F., Kappler, U., and Enemark, J. H. (2009) Exchangeable Oxygens in the Vicinity of the Molybdenum Center of the High-pH Form of Sulfite Oxidase and Sulfite Dehydrogenase. *Phys. Chem. Chem. Phys. 11*, 6733–6742.
59. Astashkin, A. V., Neese, F., Raitsimring, A. M., Cooney, J. J., Bultman, E., and Enemark, J. H. (2005) Pulsed EPR Investigations of Systems Modeling Molybdenum Enzymes: Hyperfine and Quadrupole Parameters of oxo-^{17}O in $[Mo^{17}O(SPh)_4]^-$. *J. Am. Chem. Soc. 127*, 16713–16722.
60. Betts, R. H., and Voss, R. H. (1970) The Kinetics of Oxygen Exchange Between the Sulfite Ion and Water. *Can. J. Chem. 48*, 2035–2041.
61. Enemark, J. H., Raitsimring, A. M., Astashkin, A. V., and Klein, E. L. (2010) Implications for the Mechanism of Sulfite Oxidizing Enzymes from Pulsed EPR Spectroscopy and DFT Calculations for "Difficult" Nuclei. *Faraday Discuss. 148*, (in press).
62. Workun, G. J., Moquin, K., Rothery, R. A., and Weiner, J. H. (2008) Evolutionary Persistence of the Molybdopyranopterin-Containing Sulfite Oxidase Protein Fold. *Microbiol. Mol. Biol. Rev. 72*, 228–248.
63. Kappler, U. (2008) Bacterial Sulfite-Oxidizing Enzymes: Enzymes for Chemolithotrophs Only? In Microbial Sulfur Metabolism (Dahl, C., and Friedrich, C. G., Eds.) pp 152−169, Springer, Berlin.
64. Brokx, S. J., Rothery, R. A., Zhang, G., Ng, D. P., and Weiner, J. H. (2005) Characterization of an *Escherichia coli* Sulfite Oxidase Homologue Reveals the Role of a Conserved Active Site Cysteine in Assembly and Function. *Biochemistry 44*, 10339–10348.
65. Pacheco, A., Hazzard, J. T., Tollin, G., and Enemark, J. H. (1999) The pH Dependence of Intramolecular Electron Transfer Rates in Sulfite Oxidase at High and Low Anion Concentrations. *J. Biol. Inorg. Chem. 4*, 390–401.
66. Hurley, J. H., Dean, A. M., Sohl, J. L., Koshland, D. E., and Stroud, R. M. (1990) Regulation of an Enzyme by Phosphorylation at the Active Site. *Science 249*, 1012–1016.
67. Tollin, G., Hurley, J. K., Hazzard, J. T., and Meyer, T. E. (1993) Use of Laser Flash Photolysis Time-Resolved Spectrophotometry to Investigate Interprotein and Intraprotein Electron Transfer Mechanisms. *Biophys. Chem. 48*, 259–279.
68. Tollin, G. (1995) Use of Flavin Photochemistry to Probe Intraprotein and Interprotein Electron Transfer Mechanisms. *J. Bioenerg. Biomembr. 27*, 303–309.
69. Tollin, G. (2001) in Electron Transfer in Chemistry (Balzani, V., Ed.) Vol. IV, pp 202−231, Wiley-VCH, Weinheim, Germany.
70. Feng, C., Kedia, R. V., Hazzard, J. T., Hurley, J. K., Tollin, G., and Enemark, J. H. (2002) Effect of Solution Viscosity on Intramolecular Elelctron Transfer in Sulfite Oxidase. *Biochemistry 41*, 5816–5821.
71. Kawatsu, T., and Beratan, D. N. (2006) Electron Transfer Between Cofactors in Protein Domains Linked by a Flexible Tether. *Chem. Phys. 326*, 259–269.
72. Pushie, M. J., and George, G. N. (2010) Active-Site Dynamics and Large-Scale Domain Motions of Sulfite Oxidase: A Molecular Dynamics Study. *J. Phys. Chem. B 114*, 3266–3275.
73. Utesch, T., and Mroginski, M. A. (2010) Three-Dimensional Structural Model of Chicken Liver Sulfite Oxidase in its Activated Form. *J. Phys. Chem. Lett. 1*, 2159–2164.
74. Johnson-Winters, K., Nordstrom, A. R., Davis, A. C., Tollin, G., and Enemark, J. H. (2010) Effects of Large Scale Amino Acid Substitution in the Polypeptide Tether Connecting the Heme and Molybdenum Domains on Catalysis in Human Sulfite Oxidase. *Metallomics* (in press).

75. Rajagopalan, K. V. (1980) Sulfite Oxidase (Sulfite:Ferricytochrome c Oxidoreductase). In Molybdenum and Molybdenum-Containing Enzymes (Coughlan, M. P., Ed.) 1st ed., Pergamon Press, Oxford, U.K.
76. Byrne, R. S., Hansche, R., Mendel, R. R., and Hille, R. (2009) Oxidative Half-reaction of *Arabidopsis thaliana* Sulfite Oxidase: Generation of Superoxide by a Peroxisomal Enzyme. *J. Biol. Chem. 284*, 35479–35484.
77. Spence, J. T., Kipke, C. A., Enemark, J. H., and Sunde, R. A. (1991) Stoichiometry of Electron Uptake and the Effect of Anions and pH on the Molybdenum and Heme Reduction Potentials of Sulfite Oxidase. *Inorg. Chem. 30*, 3011.
78. Elliott, S. J., McElhaney, A. E., Feng, C., Enemark, J. H., and Armstrong, F. A. (2002) A Voltammetric Study of Interdomain Electron Transfer within Sulfite Oxidase. *J. Am. Chem. Soc. 124*, 11612–11613.
79. Johnson-Winters, K., Nordstrom, A. R., Emesh, S., Astashkin, A. V., Rajapakshe, A., Berry, R. E., Tollin, G., and Enemark, J. H. (2010) Effects of Interdomain Tether Length and Flexibility on the Kinetics of Intramolecular Electron Transfer in Human Sulfite Oxidase. *Biochemistry 49*, 1290–1296.
80. Berry, R. E., Shokhireva, T. K., Filippov, I., Shokhirev, M. N., Zhang, H., and Walker, F. A. (2007) Effect of the N-Terminus on Heme Cavity Structure, Ligand Equilibrium, Rate Constants, and Reduction Potentials of Nitrophorin 2 from *Rhodnius prolixus*. *Biochemistry 46*, 6830–6843.
81. Ding, X. D., Weichsel, A., Andersen, J. F., Shokhireva, T. K., Balfour, C., Pierik, A. J., Averill, B. A., Montfort, W. R., and Walker, F. A. (1999) Nitric Oxide Binding to the Ferri- and Ferroheme States of Nitrophorin 1, a Reversible NO-Binding Heme Protein from the Saliva of the Blood-Sucking Insect, *Rhodnius prolixus*. *J. Am. Chem. Soc. 121*, 128–138.
82. Aguey-Zinsou, K.-F., Bernhardt, P. V., Kappler, U., and McEwan, A. G. (2003) Direct Electrochemistry of a Bacterial Sulfite Dehydrogenase. *J. Am. Chem. Soc. 125*, 530–535.
83. Friedrichs, M. S., Eastman, P., Vaidyanathan, V., Houston, M., Legrand, S., Beberg, A. L., Ensign, D. L., Bruns, C. M., and Pande, V. S. (2009) Accelerating Molecular Dynamic Simulation on Graphics Processing Units. *J. Comput. Chem. 30*, 864–872.
84. Goldfarb, D., Lipkin, Y., Potapov, A., Gorodetsky, Y., Epel, B., Raitsimring, A. M., Radoul, M., and Kaminker, I. (2008) HYSCORE and DEER with an Upgraded 95 GHz Pulse EPR Spectrometer. *J. Magn. Reson. 194*, 8–15.
85. Wilson, J. J., and Kappler, U. (2009) Sulfite Oxidation in *Sinorhizobium meliloti*. *Biochim. Biophys. Acta 1787*, 1516–1525.